PIV flow measurements for a rotating square smooth channel heated by basically uniform heat flux

Ruquan You[a], Haiwang Li[a,], Hongwei Wu[b], Zhi Tao[a]

[a] *National Key Laboratory of Science and Technology on Aero Engines Aero-thermodynamics, The Collaborative Innovation Center for Advanced Aero-Engine of China, Beihang University, Beijing 100191, China*
[b] *School of Engineering and Technology, University of Hertfordshire, College Lane Campus, Hatfield AL10 9AB, United Kingdom*

a b s t r a c t In this paper, we experimentally investigated the mainstream and secondary flow in a smooth rotating channel with wall heated by particle image velocimetry (PIV). The hybrid effect of Coriolis force and buoyancy force on the mainstream and secondary flow was taken into consideration in the current work. In the experiments, the Reynolds number, based on the channel hydraulic diameter (D = 80 mm) and the bulk mainstream velocity (V_m = 1.82 m/s), is 10,000, and the rotation numbers are 0, 0.13, 0.26, 0.39, respectively. Constant heat flux on the four channel walls are provided by Indium Tin Oxide (ITO) heater glass, the density ratio (d.r.) equaling approximately 0.1. The buoyancy number ranges from 0 to 0.153. The results showed that Coriolis force and buoyancy force have important influences on the flow field in rotating channels. Coriolis force pushes the mainstream to trailing side, making an asymmetry of the mainstream. On the cross-section, there is a symmetric two-vortex pair caused by the Coriolis. The two-vortex pair is pushed into the trailing side with the increase of rotation numbers. Then, there are two small vortex appearing near the leading side. Buoyancy force suppresses mainstream and causes the separation of the flow near the leading side. When the separated flow happened, the structure of sec- ondary flow is disordered near the leading side.

Keywords: Rotating channel Secondary flow Flow dynamics Heat transfer Separated flow

1. Introduction

Internal cooling technology is one of the most difficult task in gas turbine blades. Over the past several decades, a vast amount of studies dealing with internal cooling of turbine blades have been reviewed by Han and Huh [1]. However, limited by the complex measurement technology under rotating conditions, most of the experimental investigations focused on the heat transfer instead of the velocity measurement. In rotating channels, Coriolis force and buoyancy force are two important forces that affect the flow behavior and heat transfer significantly.

In rotating channels, Coriolis force pushes mainstream to trail- ing side and induces secondary flow. The direction of buoyancy force is opposite to the direction of fluid in a rotating channel. The mechanism of the flow field in a rotating channel is important for engine designers. Many investigators have studied the flow field in rotating channels experimentally. However, many investi- gators studied the mainstream field without wall heated, which mainstreams only Coriolis force was considered. In recent years,

buoyancy force begins to be taken into consideration on flow field in rotating channels because that buoyancy force has changed the flow and heat transfer distribution in rotating channels. We divided the published work focusing on mainstream and secondary flow in rotating channels into three parts:

1.1. Effect of Coriolis force on mainstream

Coriolis force is generated by rotation, the effect of which can be measured by the rotation number:

$$Ro = \frac{\Omega D}{V_m} \tag{1}$$

where Ω is the rotating speed, D is the hydraulic diameter, and V_m is the average bulk flow velocity.

The effect of Coriolis force was numerically investigated in Refs. [2,3], and experimentally investigated in Refs. [4–10]. Both of investigators found that the mainstream velocity profile is pushed to trailing side by Coriolis force, and the turbulent Reynolds stres- ses are asymmetric. They also found that rotation stabilizes the flow on leading side and destabilizes the flow on trailing side. They reported that, on the stabilized layer, the turbulent stress

decreases, which is also found by Hart [11]. Cheah et al. [12] measured the main flow at symmetry plane of the U-ducts by LDV (Laser Doppler Velocimetry) under rotating condition, and they obtained the same impact of the Coriolis force on the mainstream with Andersson, Johnson and Hart. The effect of rotation was also carried out by measuring pressure drop in a rotating duct [13], and the results show that the friction coefficient increases with rotation numbers. Liou et al. [14] used LDV to conduct the spectral analysis of flow field in a rotating duct. They found that Coriolis force promotes mixture of core and near-wall fluids. Visscher and Andersson [15] using PIV measured the separated turbulent flows with rotation. The length of the primary separation bubble decreases monotonically with the increase of rotation on leading side. Gallo and Astarita [16], Sante and Braembussche [17] all investigated the mainstream field in rotating channels. Gallo performed a reconstruction and vertical field of the mainstream to study the influence of rotation by PIV. Sante also presented a quasi-3D view of flow to illustrate the impact of Coriolis force in a rotating channel, using TR-PIV (time resolved particle image velocimetry). They found that the boundary layer thickness increases on the leading side and decreases on the trailing side. The turbulence intensity moves away from the leading side and remains close to the trailing side. They also found the hairpin vortices on the trailing side at the mid-channel planes.

1.2. Effect of Coriolis force on secondary flow

When the channel is rotating, secondary flow will be generated in the cross-section, which is an important factor affecting the flow and heat transfer in the channel.

Nandakumar et al. [18], Iacovides and Launder [19] investigated the secondary flow numerically in rotating channels, respectively. Nandakumar et al. found four vortices in the cross section, and the structure of vortices changes with the rotation numbers. While Iacovides and Launder found two small vortices in the cross section on the trailing side. Iacovides and Launder also found that Nusselt number increases on trailing side. Secondary flow was investigated using PIV by Gallo [20] and Elfert [21]. In Ref. [21], investigators compared the flow field data with heat transfer data, and identified several connections between Nu/Nu_0 and two fluid dynamics quantities turbulent kinetic energy (TKE) and normal-to wall velocity component (w). They found that with the increase of TKE, the heat transfer increases. Elfert presented secondary flow at different positions to explain the effect of rotation. Macfarlane and Joubert

[22] studied the effect of secondary flow on developing turbulent boundary layers under rotating conditions. They presented the experimental results about the interaction between secondary flows and developing rotating turbulent boundary layers, and found that the boundary layer is initially subject only to the effects of the Coriolis, then the specific effects of the secondary flows are observed. And the shear stress intensities are the most sensitive to secondary flows.

1.3. Effect of buoyancy force on mainstream and secondary flow

Buoyancy force is another important force in a rotating channel, which is induced by the temperature gradient near the wall. Buoyancy force has an important influence on the characteristics of flow and heat transfer. For a radial outward channel, buoyancy force is in the opposite direction to the direction of mainstream, suppressing the flow field near the leading side. The dimensional parameter characterizing the effect of rotation is buoyancy number:

$$Buo = Ro^2 \frac{r}{D} \frac{T_w - T_f}{T^w} \qquad (2)$$

where r is the rotating radius, T_W is the wall temperature, and T_f is the temperature of fluid. With the increase of rotating radius, the effect of rotation buoyancy force is enhanced. Siegel [23] studied the buoyancy effect on heat transfer in a rotating tube by CFD, and found that buoyancy tends to improve heat transfer at the radial inward pass and reduce heat transfer at the radial outward pass. The buoyancy force is generated by the heated wall, which mainstreams that the condition of the heated walls will affect the buoyancy force. The results is confirmed by Han and Zhang's [24] experiments. They [24] investigated the effect of uneven wall temperature on local heat transfer with various thermal boundary conditions: (A) four walls with uniform temperature, (B) four walls with uniform heat flux and (C) leading and trailing walls hot and two side cold. The investigation showed that the value of Nu/Nu_0 on the leading side for three cases is case B > case C > case A, and on the trailing side is case A > case C > case B. However, on the trailing side the differences of Nu/Nu_0 among the three cases decreases compared with those on leading side. The results they obtained suggest that the local uneven wall temperature creates the local buoyancy forces, which changes the effect of the rotation. Therefore, the local heat transfer coefficients are altered on the leading, trailing and side surfaces. Han and Dutta [25] continued their investigation by predicting the flow field in a rotating channel with Coriolis force

and buoyancy force using a two-equation turbulent model. They found a flow separation at the leading wall, and explained it with a non-dimensionless parameter that characterized an adverse buoyancy force. They found viscous force is another force in the boundary layer. When the buoyancy force is higher than viscous force, separated flow happens. Lin et al. [26] carried out a numerical study of flow and heat transfer in a smooth and ribbed U-Duct with and without rotation. They obtained the detailed structure of the secondary flow in first passage at rotating conditions, and found that secondary flow has pronounced effect on the heat transfer in rotating channel. Coriolis, centrifugal force and pressure gradient are used to explain the flow structure they have found. Bons [27] firstly experimentally investigated the effect of Coriolis force and buoyancy force in a rotating smooth channel by PIV and IR (infrared detector). However, he did not obtain the velocity data within the boundary layer, which is very important to verify results obtained by Han and Dutta by CFD. Li et al. [28,29] investigated the heat transfer in a rotating channel, they obtained that Coriolis force and buoyancy force have an important effect on leading and trailing side. Shen et al. [30] numerically studied the flow field and heat transfer in U-shaped channel with the combination of ribs, dimples and protrusions. They found that, the structures arranged on the wall surface enhanced the heat transfer in the channel. Recent years, Coletti et al. [31–33] from VKI investigated the characterization of flow in a rotating channel with the effect of buoyancy force by TR-PIV. Buoyancy force plays a major role along the leading side, and stabilizes the vortices close to the leading edge, resulting in large characteristic length and time scales, which is critical for the turbulent transport and heat transfer. However, in their experiment, only one measured wall was heated, while the other three walls were cold. The thermal boundary condition is not same as a real engine blade with four wall heated, which has a significant effect on the flow and heat transfer [24].

The investigations about the flow dynamics under the effect of Coriolis force are available, and several investigations focused on the heat transfer with the effect of buoyancy force. However, only few of the investigations studied the flow dynamics with the effect of Coriolis force and buoyancy force at the same time experimentally, which makes significant sense to understand the mechanism of flow and heat transfer in a real turbine blade coolant channel. For the mainstream, velocity profile and Reynolds shear stress with wall heated on the center plane is discussed in our previous work [34], and separated flow is captured near the leading side. For the secondary flow, two-vortex pair is obtained without wall heated in our another work [35]. What is the structure of secondary flow when the separated flow happens? As a series of research on this field, the present work focuses on the mainstream and secondary flow in a smooth rotating channel with wall heated using PIV. Reconstruction of mainstream and secondary flow are presented to explain the mechanism of flow dynamics under the effect of Coriolis force and buoyance force in the current work. What's more, the experimental data obtained in current work can also be used for CFD comparison.

2. Experimental set-up and measure procedure

2.1. Rotating facilities

The experiments present herein were performed on the advanced flow and heat transfer rotating facility, which has been mentioned in Ref. [34]. For the purpose of completeness, the rotating facility will be briefly introduced herein.

The rotating facility consists of a rotating disk, where all test sections and data acquisition modules are mounted. Extension of the rotating arms are used to make the total length of the rotating

radius can be up to 0.98 m. The rotating frame is driven by a DC motor. The coolant air, provided by a blower, passes through the flow meter, rotary joint, settle chamber (Screen & Honeycomb), and then enters into the test section. Before entering the flow meter, the seeding (provided by a Laskin-nozzle-based seeding generator) are added to the mainstream, which is used for PIV measurement. A balance weight is on the opposite side of the disk to ensure the balance of the rotating system. Thermocouples are used for measuring the temperature on the rotating frame. All the cold ends of thermocouples are placed on the aluminum-made rotating disk. Due to the good performance of thermal conductivity of aluminum, the temperature of the disk is relatively constant and even. The absolute temperature of the rotating disk is measured by a thermal resistance. The analog signals of the thermocouple are converted into digital ones before transmitted to the non-rotating facilities by signal slip rings. The heating slip ring is used for conveying the current (up to 2 A) for heating the channel.

The schematic of the rotating facility and the layout of PIV can be seen in Fig. 1. Mainstream and secondary flow field are obtained by mainstreams of PIV system. The camera is putted under the test channel and at the outside position of channel when we measure the mainstream and secondary flow, respectively. Due to the PIV system is putted out of the rotating facility, the camera is synchronized by a high accuracy FPGA module.

2.2. Test section

Fig. 2 shows the sketch of the test section. The test section has a square cross-section with dimension of D = 80 mm. The entrance of the test section has a rotating radius of 276 mm. Different with our previous work in Ref. [36], grids and trip wires are arranged at the inlet of the channel to ensure the flow is turbulent in the channle. Four 3 mm high trip wires are arranged at inside of four walls. Due to the grids and trips wires, the inlet condition in current work is different from our previous work [36] without grids and trip wires. The heated section the channel states at the trip wires, where X is defined as 0. The total length of heated region is 600 mm. The measured region of main flow in the current work are $3.5 < X/D < 6.5$, $0 < Y/D < 1$, and $0.125 < Z/D < 0.875$ with an interval of $Z/D = 0.125$. The reconstruction of the mainstream is generated by these 7 measured sections. For secondary flow, three planes are measured at the cross section of $X/D = 4, 5, 6$, respectively.

2.3. PIV setup and methodology

The velocity fields are obtained by the PIV. In the current work, the light pulses are generated by a dual-cavity 135 mJ Nd:YAG pulse laser device (532 nm) and guided via a light-guide arm to the desired test plane with a thickness of about 1 mm. The seeding is provided by a Laskin-nozzle-based seeding generator operated with DEHS, which guarantees the particle size with an average diameter of 1 lm. A digital 14 bits CCD camera (2048 × 2048 pixels²) with Nikon 105 mm macro lens is used to capture the images. Table 1 lists the magnification factors and experimental parameters used for PIV acquisition in different measured planes at different conditions.

In the current work, 500 image pairs are taken to calculate the time averaged velocity, which is enough to ensure the convergence of the results, which has been mentioned in our previous work [35]. Before process the PIV image pairs, we use the boundary of channel in the image as a mark to ensure the two image pairs at the same position, which can eliminate the effect of vibration. The collected image pairs were analyzed using the software Flow Master. In the experiments, peripheral velocity and delay time induce the movement between image pairs, and this movement induces the much larger particle displacement than a quarter of
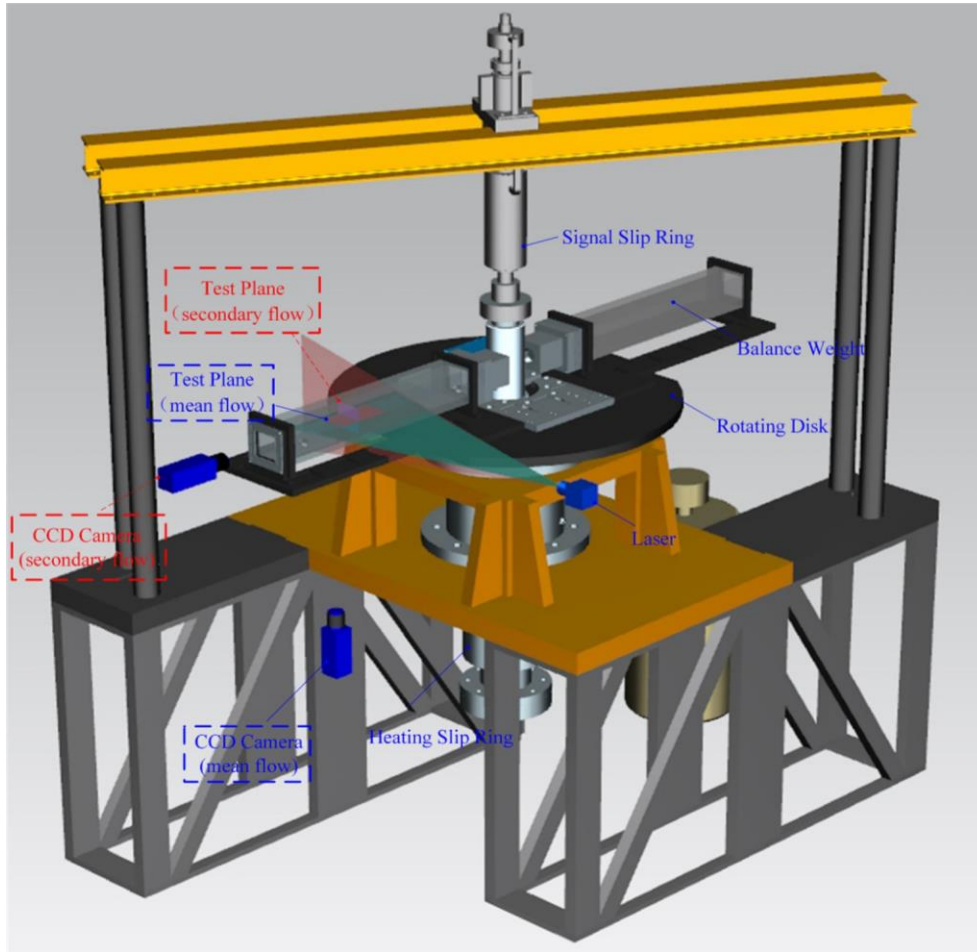
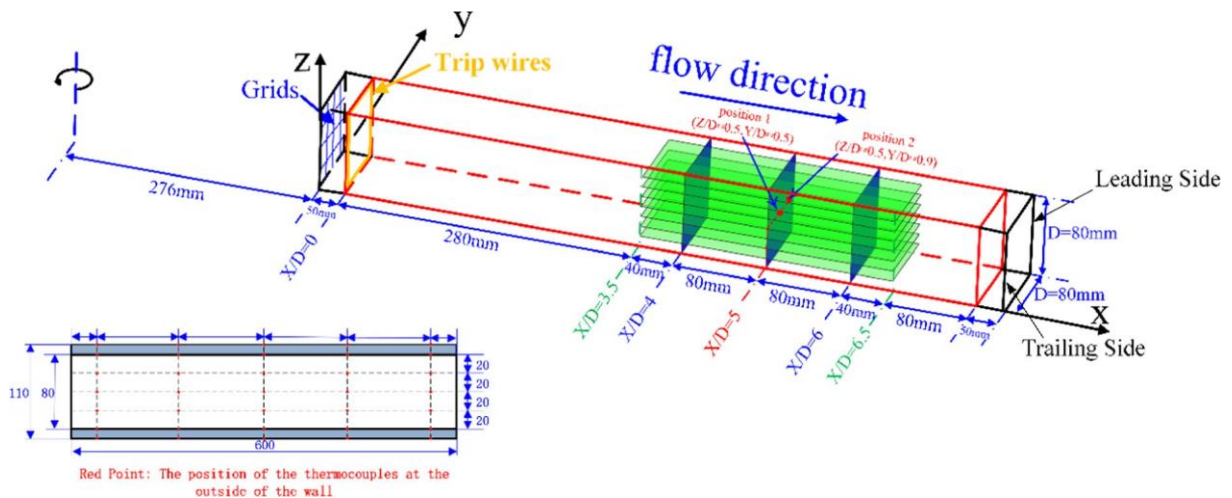Fig. 1. Rotating facility and the layout of PIV.

Fig. 2. Test section.

the interrogation region dimension. Therefore, an initial window shift is firstly used to reconstruction the image, making the displacement of the seeding particle at about 8–10 pixel. Then a flow field was calculated using the two-passes PIV interrogation algorithm and a 50% overlap. In the first pass, the dimensions of the sampling interrogation region are 64×64 pixels^2, and then changed to 32×32 pixels^2 in the second pass. Once a vector field is cal-

culated, vector validation algorithms can be applied to eliminate spurious vectors. In the present work, the peak ratio value of 2 is used as a post-processing criterion for eliminating questionable vectors below a ratio-threshold. Finally, a Gaussian peak-fitting was adopted to perform the sub-pixel interpolation to fill up the empty spaces. In current work, measured plane of the mainstream has a dimension of 80×120 mm^2, and 80×80 mm^2 of secondary

Table 1
The magnification factors and experimental parameters used for PIV acquisition.

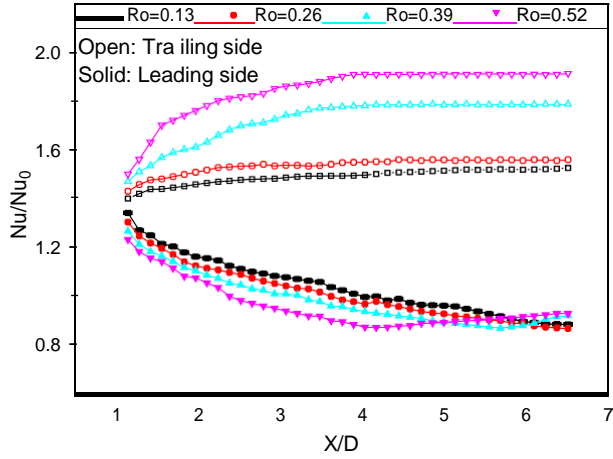| Planes	Mainstream	Secondary flow		
	(all planes)	X/D = 4	X/D = 5	X/D = 6
Magnification factor (pixel/mm)	14.92	22.72	22.57	21.92
Delay time (Dt) (■s)	200, 200, 150, 120	200, 150, 120		
Rotation speed (rpm)	0, 30, 60, 90	30, 60, 90		
Ro	0, 0.13, 0.26, 0.39	0.13, 0.26, 0.39		
Re	10,000			
Buo	0–0.15			
Image pairs	500			

Fig. 3. The distribution of Nu/Nu_0 along X/D direction at different rotation numbers with Reynolds number of 10000.

Fig. 4. Velocity profile at static conditions at X/D = 4, 5, 6 in current work with PIV.

plane. We obtained 0.92 vectors/mm of mainstream, and 1.42 vectors/mm for secondary flow.

2.4. Thermal boundary conditions

Four 1-mm-thick transparent thin film ITO (Indium Tin Oxide) heater glasses are used to provide uniform heat flux (q_{joule}) of each channel walls. To make the four walls with the same boundary thermal heat flux, four adjustable resistors are in series with each ITO heater glass to control the four walls with same heat flux, which has been introduced in detail in Ref. [37]. The q_{loss} ($q_{loss} \frac{1}{4} \frac{k_{plexis}}{d} \eth T_w - T_e \th$) is obtained by measuring the temperature of the inner channels walls (T_w) using thermochromic liquid crystal (TLCs) and the temperature of outer channels walls (T_e) by 35 thermocouples, which is presented in Fig. 2. The 1D conduction assumption of the 15 mm thick channel walls (d) is used to calculate q_{loss}. When we get the temperature of the flow (T_f), we can obtain the local heat transfer coefficient h ($h \frac{1}{4} \eth q_{joule} - q_{loss} \th = \eth T_w - T_b \th$). T_b is the local bulk temperature, which is calculated by $T_b \frac{1}{4} T_{in} \th \int \frac{q_{joule} - q_{loss}}{m \cdot C_p} \th dA$. Then Nusselt number ($Nu$) is obtained by $Nu \frac{1}{4} h = \eth k_f D \th$, where k_f is the thermal conductivity of the air flow. The uncertainty of the Nu is 6.3%. The heat flux taken away by the fluid ($q_{net} \frac{1}{4} q_w - q_{loss}$) in current work ranges from 50.582 W to 90.24 W. The inlet temperature of the fluid is controlled around 25 °C, and the total temperature increase of fluid (T_b) in the channel is no more than 5 °C from the inlet to the outlet. The temperature of the wall ranges from 40 °C to 60 °C. In the current work, the density ratio (d:r: $\frac{1}{4} \frac{T_w - T_{in}}{T_w}$, where T_w is temperature of wall, and T_{in} is the temperature of inlet fluid) is about 0.1, which makes the buoyancy number (calculated by Eq.
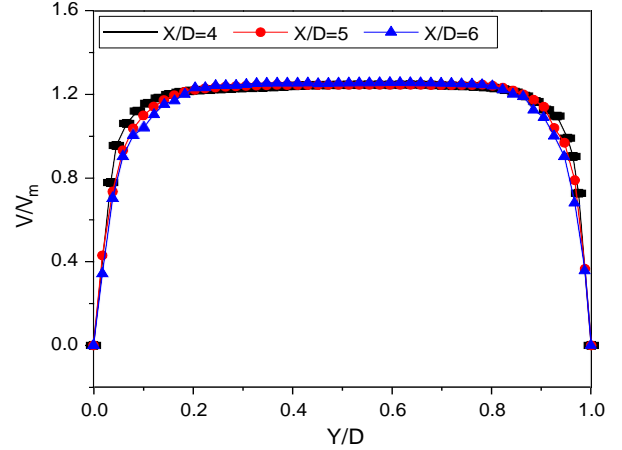
(2)) ranging from 0 to 0.153 in the current work. Fig. 3 shows the distribution of Nu/Nu_0 (Nu_0 is Nu in fully-developed turbulent flow in non-rotating smooth round pipe) along X/D direction at different rotation numbers with Reynolds number of 10,000. Since all the heated walls are transparent, the PIV measurement can be carried out.

2.5. Inlet conditions

At the inlet of the test channel, screen and honeycombs are used to smooth the inlet velocity condition. Grids and trip wires are used to ensure the fluid is turbulent. Fig. 4 presents the velocity profile (normalized by V_m) at static conditions at X/D = 4, 5, 6 in current work with PIV. According to Fig. 4, the inlet condition is smoothed very well in current work.

3. Uncertainty analysis

The total uncertainty (d; $\frac{1}{4} \sqrt{B^2 \th P^2}$) include bias uncertainty (B) and expanded uncertainty (P) [38]. The bias uncertainty in current work is the relative measurement uncertainty, which has been discussed in our previous work [34]. The bias uncertainty

Table 2
Relative measurement uncertainty of mainstream and secondary flow at different measured planes.

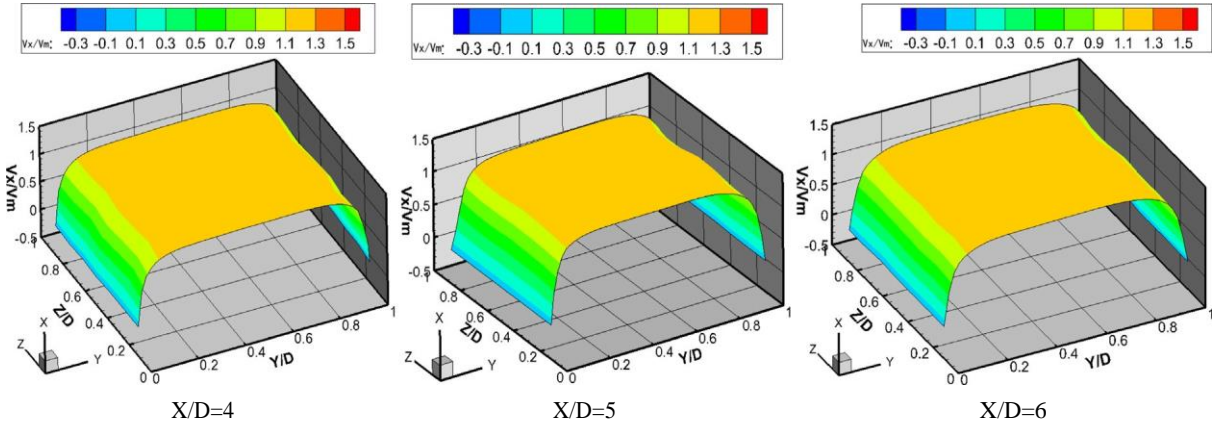| Ro	Mainstream planes	Secondary flow planes		
		X/D = 4	X/D = 5	X/D = 6
0	1.84%	–	–	–
0.13	1.84%	8.81%	11.75%	14.69%
0.26	2.45%	8.86%	11.82%	14.77%
0.39	3.06%	9.12%	12.16%	15.20%

Fig. 5. Reconstruction of mainstream field at different positions (X/D = 4, 5, 6) with wall heated experimentally at static conditions.
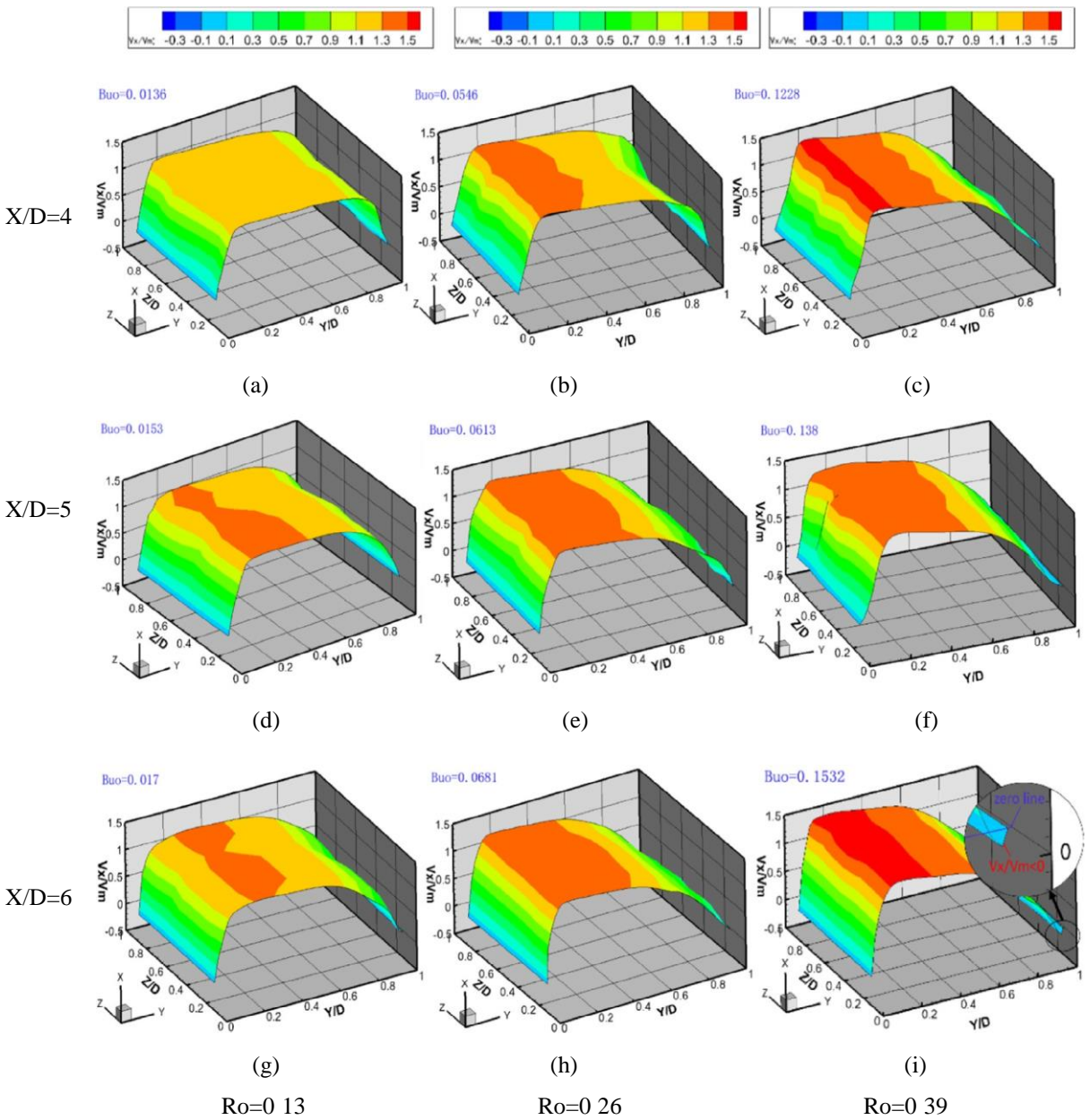

Fig. 6. Reconstruction of mainstream field at different positions (X/D = 4, 5, 6) with wall heated for different rotation numbers.
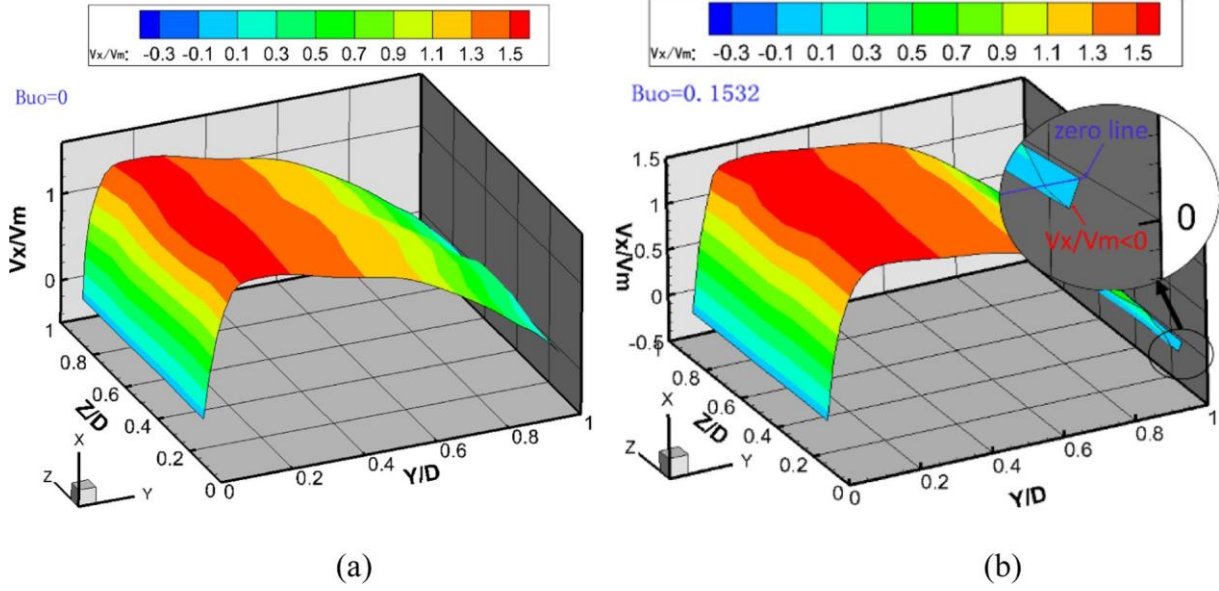
Fig. 7. Reconstruction of mainstream field at X/D = 6 without (a) and with (b) wall heated at Ro = 0.39.

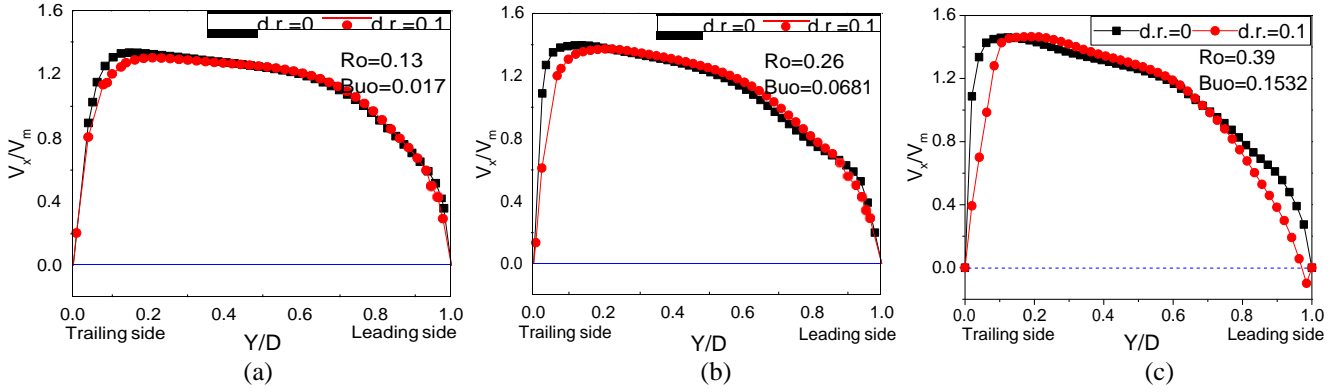Fig. 8. Comparison of velocity profile with and without wall heated at Z/D = 0.5, X/D = 6 with different rotation numbers.

$B \frac{1}{4} \left[\left(\frac{@z}{@x_1} \right)^2 (dx_1) + \cdots + \left(\frac{@z}{@x_n} \right)^2 (dx_n) \right]$, and precious uncertainty $P \frac{1}{4} \frac{tr}{P_{\frac{1}{N}}}$.

In the current work, the PIV system is arranged outside the rotating facility, the relative velocity 'V' was calculated by subtracting the peripheral velocity '$V_{rot} = Xr$' from the measured absolute velocity '$V_{abs} \frac{1}{4} \frac{DsxM}{Dt}$, where X is the rotation speed, r is the rotating radius, Ds is the particle displacement, Dt is the delay time of the image pairs, and M is the magnification factor. The error of the relative velocity depends on the error of the V_{abs} and V_{rot}, calculated by Eq. (3):

$$ dV \frac{1}{4} \left[\frac{@V}{@V_{abs}} \right]^2 (dV_{abs})^2 + \left[\frac{@V}{@V_{rot}} \right]^2 (dV_{rot})^2 \qquad (3) $$

The uncertainty of V_{rot} can be calculated by Eq. (4):

$$ dV_{rot} \frac{1}{4} \left[\frac{@V_{rot}}{@X} \right]^2 (dX)^2 + \left[\frac{@V_{rot}}{@r} \right]^2 (dr)^2 \qquad (4) $$

In current work, a FPGA based trigger signal generator is used to synchronize the PIV system, which can provide the uncertainty of the rotation speed (dX) is 0.0127 rpm. The accuracy of rotation radius (dr) is 0.1 mm.

The dV_{abs} can be calculated by Eq. (5).

$$ dV_{abs} \frac{1}{4} \left[\frac{@V_{abs}}{@Ds} \right]^2 (dDs)^2 \qquad (5) $$

In Eq. (5), $V_{abs} \frac{1}{4} \frac{DsxM}{Dt}$, where Ds is the particle displacement, Dt is the delay time of the image pairs, and M is the magnification factor. The estimated of uncertainty on PIV measurements (dDs) is 0.1 pixels following the approach made by Ref. [39].

With the mean velocity of mainstream (V_m) about 1.82 m/s, delay time and the magnification factor of different measured planes, relative measurement uncertainty (bias uncertainty [38]) for mainstream (about 2.2 m/s) and secondary flow (about 0.25 m/s) in core region can be seen calculated using Eq. (3), which can be seen in Table 2.

The expanded uncertainty $\left(P \frac{1}{4} \frac{tr}{P_{\frac{1}{N}}} \right)$ in the current work is less than 0.8% of all conditions, where t is the confidence coefficient and r is the standard deviation of the sample of N images (N = 500 in current work). According to Ref. [38], t equals 1.96 for a 95% confidence level with $N > 60$. For mainstream, the test plane is parallel to the rotation direction, particle movements mainly on the test plane, the out-of-plane loss of particles can be ignored. For secondary flow, since the mainstream velocity is vertical to the
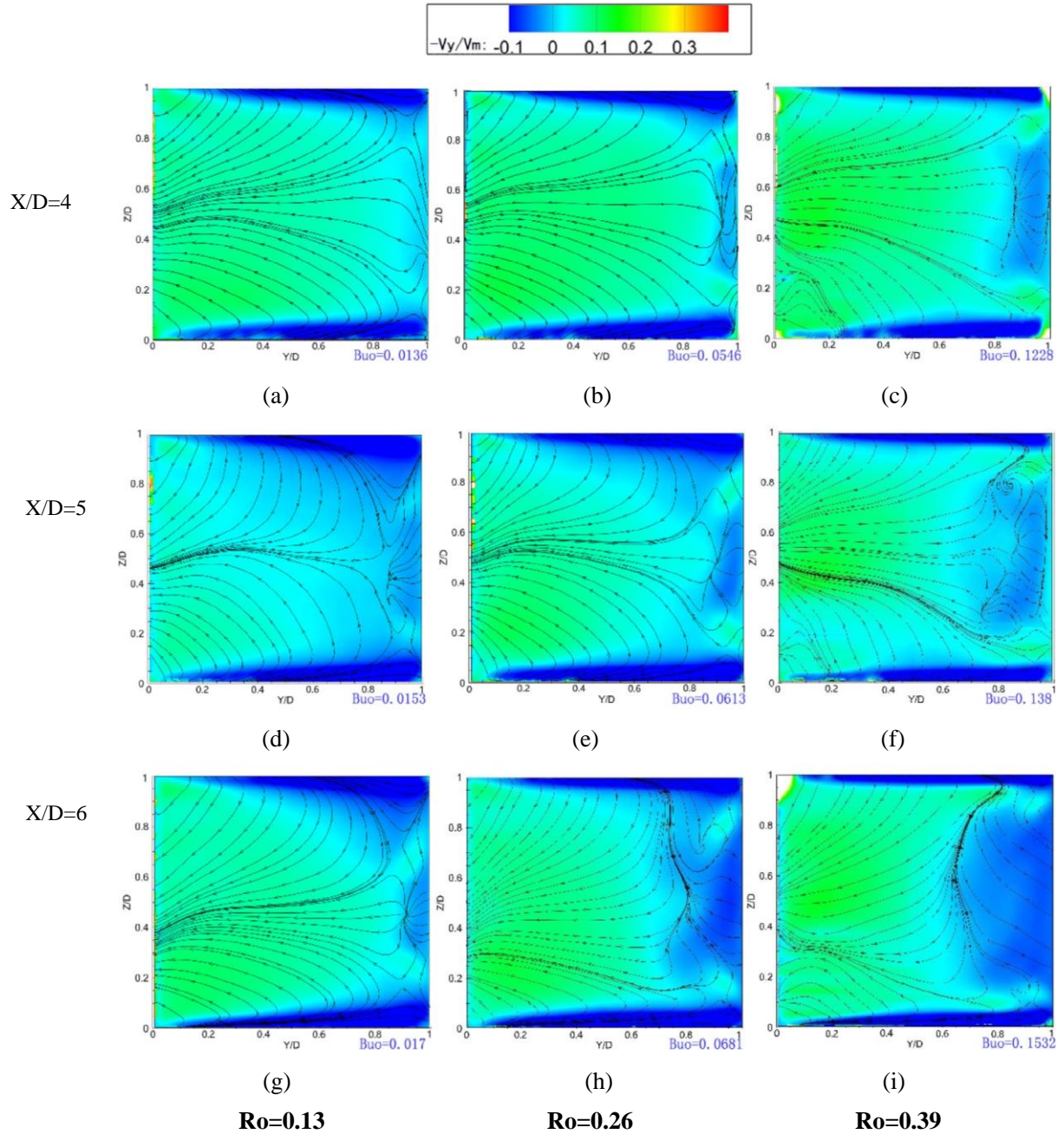
Fig. 9. Secondary flow streamlines at different position (X/D = 4, 5, 6) with wall heated for different rotation numbers.

laser sheet, we control the delay time (Δ*t*) to avoid the particles moving out of the laser light thickness (about 1 mm).

4. Result and discussion

4.1. Mainstream

For the purpose of comparison with rotating condition, the velocity component (V_x) at static conditions was measured firstly in Fig. 5 at different positions (X/D = 4, 5, 6) with wall heated. The velocity data are normalized by the mainstream bulk velocity (V_m = 1.82 m/s). The velocity distribution is well smoothed and symmetrical along the Y direction (Y/D) due to the screen and honeycombs at the inlet of the channel. Along the Z direction (Z/D), the

velocity is almost same with only a little difference causing by the fluctuation of the flow rate in different experiments.

Fig. 6 presents the reconstruction of mainstream field at different positions (X/D = 4, 5, 6) and rotation numbers (Ro = 0.13, 0.26, 0.39) with heated boundary condition. Coriolis force pushes the mainstream to the trailing side, causing the velocity profile is asymmetric. At a certain rotation number, comparing among a, d, and g, (or b, e, and h, or c, f, and i) the asymmetry of velocity profile becomes more serious along the X/D directions (a, d, g, or b, e, h, or c, f, i). This is because, with the increase of X/D, the effect of Coriolis force enhanced. Coriolis force will stabilize the boundary layer on the leading side, and causing an unstable boundary layer on the trailing side.

As mention above, when there is a temperature gradient near the wall, buoyancy force will be induced in the rotating channel.
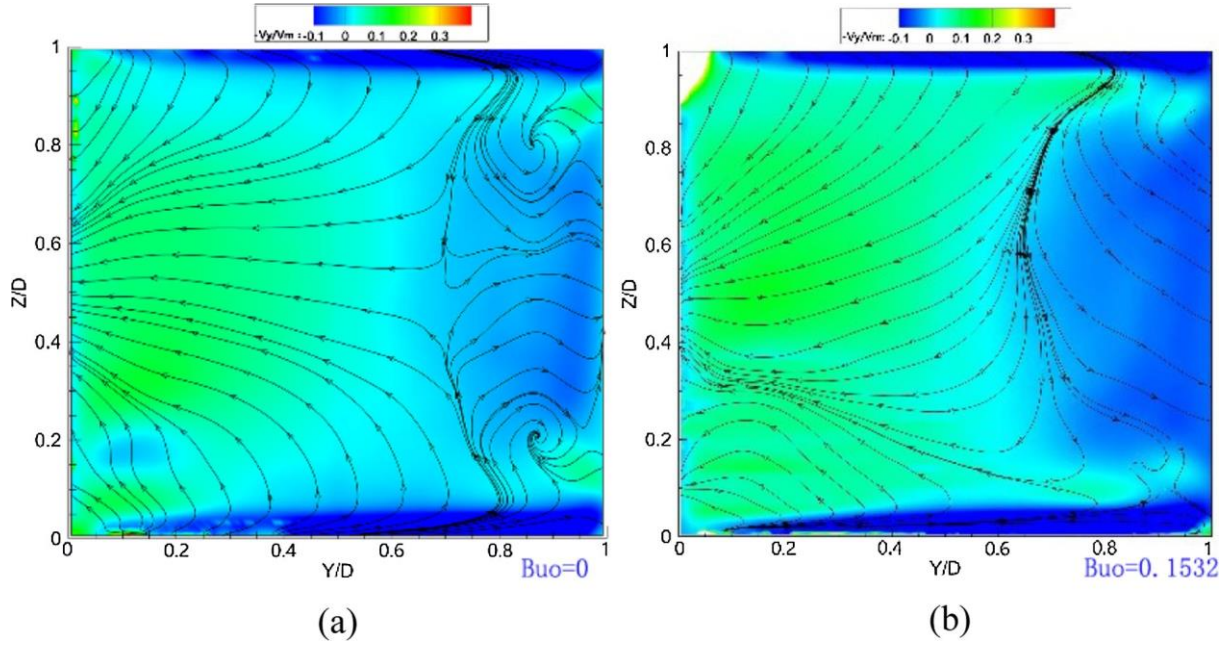
Fig. 10. Secondary flow streamlines at X/D = 6 without (a) [35] and with (b) wall heated with Ro = 0.39.
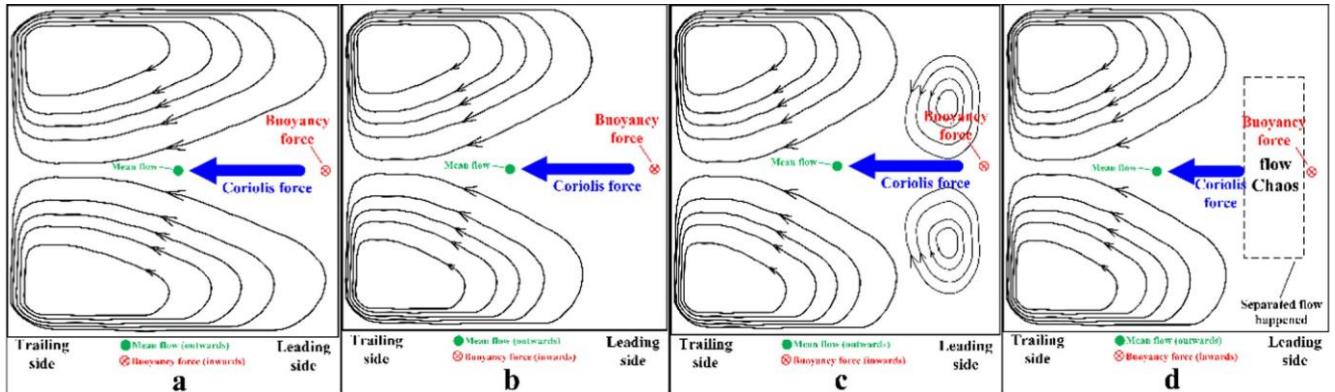

Fig. 11. Sketch of the secondary flow in rotating channels with wall heated.

Buoyancy number (Buo) is a parameter characterizing the effect of buoyancy force, which is positively related to X/D and rotation number. When the rotation number increases to 0.39 at the position of X/D = 6 (Fig. 7(i)), separated flow happens on the leading side (Y/D = 1).

To make the phenomenon more obvious, Fig. 7 shows the comparison of the mainstream field without and with wall heated at X/D = 6 and Ro = 0.39. When the wall is cold, no buoyancy force was induced, which means only Coriolis force exists. The flow field is pushed to the trailing side. While, when the wall heated, buoyancy force is induced. Comparing about Fig. 7(a) and (b), the difference is obvious on the leading side. Separated flow happened near the leading side with buoyancy force. Which means, that buoyancy force suppresses the mainstream on the leading side, and causes the separated flow. When the separated flow happens, heat transfer will be enhanced at the same position, which can be proved in Fig. 3. According to Fig. 3, on the leading side, Nu/Nu_0 is increasing along the streamwise direction on the leading side. When the rotation number up to 0.39 at the position of X/D = 6, the Nu/Nu_0 enhances at the same position.

Fig. 8 shows the comparison of velocity with and without wall heated extract from the profile of Z/D = 0.5, X/D = 6 with different rotation numbers. Comparing with the case with and without wall heated, on the trailing side, the velocity is higher in the case without wall heated than that with wall heated among three different rotation numbers. On both leading and trailing side, the velocity is also lower with wall heated than that without wall heated. Which can confirm that buoyancy force suppresses the flow in the boundary layer. According to Fig. 8(c), when rotation number increases up to 0.39, the velocity on the leading side is lower than zero, which mainstreams separated flow happened, which reveals the phenomenon that it is the separated flow that enhances the local heat transfer near the leading side [40].

4.2. Secondary flow

When the channel is rotating, secondary flow will be generated in the cross-section, which is an important factor affecting the flow and heat transfer in rotating channels. In our previous work [35], we have obtained the secondary flow in the same channel but

without wall heated. Since it is a series of investigation, in current work, we will present the secondary flow with the wall heated, and compare the difference between the two cases. Fig. 9 shows the secondary flow streamline at different positions (X/D = 4, 5, 6) with wall heated for different rotation numbers, respectively.

According to Fig. 9, secondary flow strongly impinges to the trailing side at the middle region of (Z=D ◆0:5). Near the leading side, secondary flow vectors are kind of chaos, and even deteriorates with the increase of rotation numbers. Near the end walls (Ekman layer near the end walls) of the cross-section, secondary vectors are all in the opposite direction of Coriolis force.

Secondary flow enhances in the whole region of cross-section, because of the increase of rotation numbers. Coriolis force pushes the mainstream into the trailing side, causing the magnitude of the velocity is lower near the leading side than that near the trailing side, and the difference enhances with the increase of rotation numbers. Along the streamwise direction, the shrinking region of secondary flow velocity near the leading side is enhanced at the same rotation number, which mainstreams the effect on secondary flow has a positive relation to X/D.

At the position of X/D = 4, we obtained a symmetric two-vortex pair in the cross section with the rotation number of 0.13 (Fig. 9 (a)). With the increase of rotation number, the two-vortex pair are pushed to the trailing side, which indicates that the Coriolis force enhanced. As mentioned above, the effect on secondary flow is enhanced with the increase of X/D, which mainstreams that, the vortex structure will be changed along the streamwise direction. At the position of X/D = 5, when the rotation number up to 0.39 (Fig. 9 (f)), there are two small vortex generated near the leading side. While on the position of X/D = 6, the streamline on the leading side is disordered with the rotation number of 0.39 (Fig. 9(i)). We attribute this phenomenon to the separated flow happened on the leading side. According to Fig. 6(i), separated flow happens near the leading side at the position of X/D = 6 with the rotation number of 0.39. When separated flow occurs, mainstream reversed near the leading side, causing the secondary flow disordered. To validate this, we compare the vortex structure in the case with and without buoyancy force.

Fig. 10 presents the comparison of the secondary flow in our previous work [35] without wall heated (a) with current work with wall heated (b) at X/D = 6 with Ro = 0.39. In the case without wall heated, vortex structure on the cross-section plane is a symmetric two-vortex pair near the trailing side, and two small vortexes near the leading side. While in the case with buoyancy force, the streamline is not symmetric in the plane of cross-section. There are still a two-vortex pair near the trailing side, but streamline is chaos near the leading side. The different structure between the case with and without buoyancy force confirmed that buoyancy force has a significant effect on secondary flow. As mentioned above, in the case with wall heated, buoyancy force causing separated flow near the leading side, which results in the chaos flow of the secondary flow near the leading side.

Secondary flow is an important factor affecting the flow and heat transfer in rotating channels [20], the structure of which is influenced by rotation numbers and wall thermal conditions. In the current work, we given the sketch of the secondary flow in rotating channels with wall heated in Fig. 11. In the case with low rotation number (Fig. 11(a), correspond with Fig. 10(a)), there is a symmetric two-vortex pair on the cross-section plane. With the increase of rotation numbers (Fig. 11 b, correspond with Fig. 10(b) –(e) and (g)), the two-vortex pair is pushed into the trailing side. Then, two small vortex appears near the leading side (Fig. 11 c, correspond with Fig. 10(f) and (h)). When the separated flow happens, secondary flow is disordered near the leading side (Fig. 11 d, correspond with Fig. 10(i)), which is due to the effect of buoyancy force.

5. Conclusions

Mainstream and secondary flow were investigated experimentally in a smooth rotating channel with buoyancy force by PIV measurement. Experiments were performed in a constant Reynolds number of 10,000, and a comprehensive rotation number, ranging from 0 to 0.39. Four channel walls are heated with Indium Tin Oxide (ITO) heater glass, making the density ratio (d.r.) at about 1.1. Mainstream field was performed a reconstruction at the position of 3.5 < X/D < 6.5, 0 < Y/D < 1, and 0.125 < Z/D < 0.875. Secondary flow is measured on the cross section with 0 < Y/D < 1 and 0 < Z/D < 1, at the position of X/D = 4, 5, 6, respectively. The following are the main conclusion reached.

(1) Reconstruction of mainstream and secondary flow with wall heated are firstly presented with wall heated experimentally to reveal the mechanism of heat transfer in a rotating channel. With the increase of buoyancy force, separated flow happens near the leading side, causing the Nu/Nu_0 enhanced at the certain position.

(2) Secondary flow is enhanced with the increase of rotation number and stream wise directions (X/D). Coriolis force pushes the mainstream to the trailing side, therefore, the magnitude of the secondary flow vector is lower near the leading side than that near the trailing side.

(3) In the cross-section plane, the structure of secondary flow is influenced by Coriolis and buoyancy force. There is a symmetric two-vortex pair at a low rotation number (Ro = 0.13). Then the two-vortex pair is pushed into the trailing side with the increase of rotation numbers, and two small vortex appears near the leading side. When the separated flow happened, secondary flow is disordered near the leading side.

Conflict of interest statement

We declare that we have no conflict of interest.

References

[1] J.C. Han, M. Huh, Recent studies in turbine blade internal cooling, Heat Transf. Res. 41 (2010) 803–828.
[2] R. Kristoffersen, H.I. Andersson, Direct simulations of low-Reynolds-number turbulent flow in a rotating channel, J. Fluid Mech. 256 (1993) 163–197.
[3] H.S. Kheshgi, L.E. Scriven, Viscous flow through a rotating square channel, Phys. Fluids 28 (1985) 2968–2979.
[4] T.M. Liou, M.Y. Chen, Y.M. Wang, Heat transfer, fluid flow, and pressure measurements inside a rotating two-pass duct with detached 90-deg ribs, J. Turbomach. – Trans. ASME 125 (2003) 565–574.
[5] T.M. Liou, Y.Y. Wu, Y. Chang, LDV Measurements of periodic fully developed main and secondary flows in a channel with rib-disturbed walls, J. Fluids Eng. 115 (1993) 109–114.
[6] T.M. Liou, S.W. Chang, J.H. Hung, S.F. Chiou, High rotation number heat transfer of a 45° rib-roughened rectangular duct with two channel orientations, Int. J. Heat Mass Transf. 50 (2007) 4063–4078.
[7] T.M. Liou, C.C. Chen, M.Y. Chen, TLCT and LDV measurements of heat transfer and fluid flow in a rotating sharp turning duct, Int. J. Heat Mass Transf. 44 (2001) 1777–1787.
[8] J.P. Johnston, Effects of system rotation on turbulence structure: a review relevant to turbomachinery flows, Int. J. Rotating Mach. 4 (1998) 97–112.
[9] J. Wagner, B. Johnson, Heat transfer in rotating passages with smooth walls and radial outward flow, J. Turbomach. 113 (1991) 42–51.
[10] J.P. Johnston, R.M. Halleent, D.K. Lezius, Effect of spanwise rotation on the structure of two-dimensional fully developed turbulent channel flow, J. Fluid Mech. 56 (1972) 533–557.

[11] J.E. Hart, Instability and secondary motion in a rotating channel flow, J. Fluid Mech. 45 (1971) 341–351.

[12] S.C. Cheah, H. Iacovides, D.C. Jackson, H. Ji, B.E. Launder, LDA investigation of the flow development through rotating U-ducts, J. Turbomach. – Trans. ASME 118 (1996) 590–596.

[13] G. Mårtensson, J. Gunnarsson, A. Johansson, H. Moberg, Experimental investigation of a rapidly rotating turbulent duct flow, Exp. Fluids 33 (2002) 482–487.

[14] T.-M. Liou, M.-Y. Chen, K.-H. Chang, Spectrum analysis of fluid flow in a rotating two-pass duct with detached 90° ribs, Exp. Therm. Fluid Sci. (2003).

[15] J. Visscher, H.I. Andersson, Particle image velocimetry measurements of massively separated turbulent flows with rotation, Phys. Fluids 23 (2011).

[16] M. Gallo, T. Astarita, 3D reconstruction of the flow and vortical field in a rotating sharp "U" turn channel, Exp. Fluids 48 (2010) 967–982.

[17] A. Di Sante, R.A. den Braembussche, Experimental study of the effects of spanwise rotation on the flow in a low aspect ratio diffuser for turbomachinery applications, Exp. Fluids (2010).

[18] K. Nandakumar, H. Raszillier, F. Durst, Flow through rotating rectangular ducts, Phys. Fluids A Fluid Dyn. 3 (1991) 770–781.

[19] H. Iacovides, B.E. Launder, Parametric and numerical study of fully-developed flow and heat transfer in rotating rectangular ducts, in: ASME, 35th International Gas Turbine and Aeroengine Congress and Exposition, 1990, pp. 331–338.

[20] M. Gallo, T. Astarita, G.M. Carlomagno, Thermo-fluid-dynamic analysis of the flow in a rotating channel with a sharp "U" turn, Exp. Fluids 53 (2012) 201–219.

[21] M. Elfert, M. Schroll, W. Forster, PIV measurement of secondary flow in a rotating two-pass cooling system with an improved sequencer technique, J. Turbomach. – Trans. ASME 134 (2012).

[22] I. Macfarlane, P.N. Joubert, Effects of secondary fows on developing, turbulent, rotating boundary layers, Exp. Therm. Fluid Sci. (1998).

[23] R. Siegel, Analysis of buoyancy effect on fully developed laminar heat transfer in a rotating tube, J. Heat Transf. 107 (1985) 338–344.

[24] J.-C. Han, Y. Zhang, Effect of uneven wall temperature on local heat transfer in a rotating square channel with smooth walls and radial outward flow, J. Heat Transf. 114 (1992) 850–858.

[25] S. Dutta, M.J. Andrews, J.-C. Han, Prediction of turbulent heat transfer in rotating smooth square ducts, Int. J. Heat Mass Transf. 39 (1996) 2505–2514.

[26] Y.L. Lin, T.I.P. Shih, M.A. Stephens, M.K. Chyu, A numerical study of flow and heat transfer in a smooth and ribbed U-duct with and without rotation, J. Heat Transf. 123 (2001) 219.

[27] J.P. Bons, Complementary Velocity and Heat Transfer Measurements in a Rotating Turbine Cooling Passage, Massachusetts Institute of Technology, 1997.

[28] H. Li, R. You, H. Deng, Z. Tao, J. Zhu, Heat transfer investigation in a rotating U-turn smooth channel with irregular cross-section, Int. J. Heat Mass Transf. 96 (2016) 267–277.

[29] Y. Li, H. Deng, Z. Tao, G. Xu, Y. Chen, Heat transfer characteristics in a rotating trailing edge internal cooling channel with two coolant inlets, Int. J. Heat Mass Transf. 105 (2017) 220–229.

[30] Z. Shen, Y. Xie, D. Zhang, Numerical predictions on fluid flow and heat transfer in U-shaped channel with the combination of ribs, dimples and protrusions under rotational effects, Int. J. Heat Mass Transf. 80 (2015) 494–512.

[31] I. Mayo, G. Luca Gori, A. Lahalle, T. Arts, Aerothermal characterization of a rotating ribbed channel at engine representative conditions—Part I: High-resolution particle image velocimetry measurements, J. Turbomach. 138 (2016) 101008.

[32] F. Coletti, D.L. Jacono, I. Cresci, T. Arts, Turbulent flow in rib-roughened channel under the effect of Coriolis and rotational buoyancy forces, Phys. Fluids 26 (2014) 045111.

[33] F. Coletti, I. Cresci, T. Arts, Time-resolved PIV measurements of turbulent flow in rotating rib-roughened channel with coriolis and buoyancy forces, in: Proceedings of ASME Turbo Expo 2012, 2012.

[34] R. You, H. Li, Z. Tao, K. Wei, G. Xu, PIV measurements of turbulent flows in a smooth channel with the heated boundary under rotation conditions, Appl. Therm. Eng. 123 (2017) 1021–1033.

[35] R. You, H. Li, Z. Tao, Experimental investigation on two-dimensional heat transfer and secondary flow in a rotating smooth channel, Int. J. Heat Mass Transf. 113 (2017) 342–353.

[36] K. Wei, Z. Tao, H. Wu, G. Xu, H. Li, R. You, Interaction between the primary flow fields and the secondary flow fields under rotating condition, Exp. Therm. Fluid Sci. 84 (2017) 217–230.

[37] R. You, H. Li, Z. Tao, K. Wei, Heat transfer investigation in a smooth rotating channel with thermography liquid crystal, in: ASME Turbo Expo 2016: Turbomachinery Technical Conference and Exposition, American Society of Mechanical Engineers, 2016, pp. V05BT16A006–V005BT016A006.

[38] H.W. Coleman, W.G. Steele, Engineering application of experimental uncertainty analysis, AIAA J. 33 (1995) 1888–1896.

[39] J. Westerweel, Theoretical analysis of the measurement precision in particle image velocimetry, Exp. Fluids 29 (2000) S3–S12.

[40] H. Deng, L. Qiu, Z. Tao, S. Tian, Heat transfer study in rotating smooth square U-duct at high rotation numbers, Int. J. Heat Mass Transf. 66 (2013) 733–744.